Research Square

Preprints are preliminary reports that have not undergone peer review.
They should not be considered conclusive, used to inform clinical practice,
or referenced by the media as validated information.

Development and Validation of a Radiomics Nomogram Using Intratumoral and Peritumoral CT Features to Predict Lauren Classification in Gastric Cancer

Hang Xiong
Second Affiliated Hospital of Kunming Medical College
Yun Gong
Second Affiliated Hospital of Kunming Medical College
Ruitong Sun
Second Affiliated Hospital of Kunming Medical College
Shi Chen
Second Affiliated Hospital of Kunming Medical College
Yunyu Liu
Second Affiliated Hospital of Kunming Medical College
Woxin Pi
Second Affiliated Hospital of Kunming Medical College
Feng Sun
SunFeng1971@163.com

Second Affiliated Hospital of Kunming Medical College

Research Article

Keywords: Computed tomography, Gastric cancer, Lauren classification, Nomogram, Peritumoral, Radiomics

Posted Date: June 8th, 2026

DOI: https://doi.org/10.21203/rs.3.rs-9584167/v1

License: This work is licensed under a Creative Commons Attribution 4.0 International License. Read Full License

Additional Declarations: No competing interests reported.

Abstract

Background

Preoperative identification of Lauren classification is essential for optimizing therapeutic strategies in gastric cancer (GC). We developed and validated an integrated CT radiomics nomogram incorporating intratumoral and multi-distance peritumoral features (2 mm and 3 mm) to noninvasively predict Lauren types.

Methods

A total of 238 patients who underwent radical or subtotal gastrectomy were enrolled (training cohort, n = 164; validation cohort, n = 74). Radiomics features were extracted from arterial-phase CT images. Independent clinical predictors—including T stage, cholinesterase (CHE), body weight, and white blood cell (WBC) count—were selected by multivariate logistic regression. Discrimination was evaluated using the area under the receiver operating characteristic curve (AUC) and compared by DeLong tests. Calibration was assessed using the Hosmer–Lemeshow (HL) test, and clinical utility was determined by decision curve analysis (DCA).

Results

In the training cohort, the combined nomogram achieved an AUC of 0.773 (95% CI: 0.665–0.880) and significantly outperformed the clinical-only model (DeLong test, p = 0.005). In the validation cohort, performance decreased (AUC 0.5–0.6), but the combined model showed the most stable calibration (HL test) and consistent agreement between predicted and observed outcomes. DCA demonstrated the highest net benefit of the combined nomogram across a wide range of threshold probabilities. Notably, integrating peritumoral radiomics at 2 mm and 3 mm together with clinical variables, particularly T stage (OR = 3.255, p = 0.005), enhanced discriminative ability and decision-making value.

Conclusion

The proposed multi-region radiomics nomogram provides clinically useful and noninvasive preoperative prediction of Lauren classification in GC.

Introduction

Gastric cancer (GC) ranks as the fifth most common malignancy and the third leading cause of cancer-related mortality globally [1–3]. Presently, radical surgical resection remains the primary treatment modality for resectable GC [4]. Despite ongoing advancements in adjuvant therapies, the postoperative survival rate for GC remains inadequate, with a 5-year overall survival (OS) rate of merely 20%–30% [1, 5]. GC is marked by its complexity and significant heterogeneity, presenting a range of histopathological features and clinical behaviors [6, 7]. The Lauren classification system is one of the most important histological categorization methods for GC, dividing lesions into three distinct types: intestinal, diffuse, and mixed. The intestinal and diffuse types exhibit differing clinical behaviors and molecular profiles, while the clinicopathological characteristics and prognosis of the mixed type are generally similar to those of the diffuse type [8, 9]. Therefore, the Lauren classification serves as a vital prognostic indicator for patients with GC [10].

Beyond morphological disparities, these subtypes demonstrate significant molecular differences, which may explain the variations in therapeutic response and prognosis among patients with different Lauren types [11]. Evidence indicates that patients with the diffuse type may exhibit increased sensitivity to chemotherapy [12]; however, they also face relatively higher postoperative recurrence rates and a lower 5-year overall survival (OS) compared to those with the intestinal type [8, 10, 13]. Furthermore, studies have established that only patients with the intestinal type experience substantial benefits from neoadjuvant chemotherapy regarding both OS and progression-free survival (PFS) [14, 15]. In clinical practice, the Lauren classification serves as a crucial reference for customizing surgical strategies and determining the application of trastuzumab [16].

Preoperative prediction of the Lauren classification currently depends largely on endoscopy, pathological biopsy, and molecular biomarker analysis. Although endoscopy and biopsy yield definitive histological information essential for diagnosis [17], these methods are constrained by their invasiveness, the possibility of sampling errors, and contraindications in specific patient populations. Non-invasive imaging techniques are being investigated as potential alternatives for preoperative prediction; however, their clinical utility necessitates further validation [18, 19]. Consequently, precise preoperative prediction of the Lauren classification is of considerable clinical importance for enhancing prognostic systems and informing personalized treatment strategies.

In dynamic contrast-enhanced magnetic resonance imaging (DCE-MRI) of gastric cancer (GC), the extracellular-extravascular volume fraction derived from the tumor region of interest (ROI) is reported to be higher in the diffuse type than in the intestinal type [20]. However, DCE-MRI

parameters are typically assessed from an ROI on a single selected axial slice of the perfusion map, which may not adequately represent the entire tumor volume. Liu et al. [21] investigated CT-based texture analysis by extracting features from arterial and portal venous phase CT slices that display the maximum lesion area. Their results indicated that entropy and standard deviation in the arterial phase, along with maximum attenuation, mean attenuation, and various percentiles in the portal venous phase, could serve as promising non-invasive predictors. Nonetheless, variations in individual circulatory status may result in discrepancies between arterial and venous phases measured at consistent delay times, which presents challenges for clinical application. Furthermore, the study did not evaluate peritumoral characteristics, leading to an incomplete research framework.

Radiomics employs automated quantitative characterization algorithms to transform high-throughput, region-of-interest (ROI)-based image data into radiomic features that capture tumor heterogeneity and biological behavior [22, 23]. In recent years, radiomics has revealed significant potential in tumor diagnosis, prognostic prediction, and therapeutic response assessment [24–28]. Notably, advancements in radiomics have provided new insights for the personalized management of gastric cancer (GC), including the prediction of lymph node metastasis [29, 30], distant metastasis [31], treatment response [32], and prognosis [33, 34]. These studies highlight the utility of radiomics, indicating its promise as a tool for predicting the Lauren classification in GC.

To date, research on the integration of intratumoral and peritumoral CT radiomics for this purpose remains limited. In the present study, we developed and validated a radiomics nomogram that incorporates intratumoral, peritumoral, and clinical information to facilitate non-invasive preoperative prediction of Lauren classification in patients with GC.

Methods

This research examined the differences between conventional omics techniques and assessments of various peri-tumoral regions, highlighting the unique effects each has on the overall model's efficacy. The model successfully integrates imaging with molecular data, serving as a robust tool for enhancing disease prognosis and management. Figure 1 illustrates the workflow of this comprehensive methodology.

Patients

The Institutional Review Board (IRB) approved this retrospective study and waived the requirement for informed consent, ensuring that the research complied with the principles of the Declaration of Helsinki. A total of 331 patients with gastric cancer (GC) were retrospectively enrolled between December 2015 and August 2025.

The inclusion criteria were as follows: (1) All patients received a histopathological diagnosis of gastric cancer (GC) and underwent either radical gastrectomy or subtotal gastrectomy with gastrojejunostomy; (2) complete clinical and postoperative pathological information was available; (3) contrast-enhanced abdominal CT images were obtained within 15 days prior to surgery; and (4) patients had no local or systemic therapy prior to surgical intervention. The exclusion criteria included: (1) lesions that were not visible on CT images or exhibited poor image quality; (2) absence of definitive Lauren classification data; and (3) pathological stage T < 2.

Ninety-three patients were excluded for the following reasons: (a) T < 2 stage (n = 76); (b) poor image quality or lesions not visible on CT (n = 8); and (c) absence of Lauren classification information (n = 9). Ultimately, a total of 238 patients (166 males, 72 females; mean age 60.5 ± 10.65 years) were included in the final analysis (Fig. 2). All cases were stratified and randomly assigned to the training and test sets in a 7:3 ratio. In the machine learning pipeline, the Lauren diffuse and mixed types were designated as “1” (n = 192), while the intestinal type was designated as “0” (n = 46).

Image Acquisition

ROI Segmentation: In this study, regions of interest (ROIs) were manually delineated on the training dataset utilizing ITK-SNAP software (version 3.8.0). The segmentation was conducted by two experienced radiologists. Any discrepancies that arose during the annotation process were resolved through consensus with a senior radiologist possessing over 20 years of clinical expertise. This meticulous manual delineation process provided the foundational training data for the subsequent development of automated segmentation models.

Peritumoral Region Expansion: The peritumoral region, which encompasses the area immediately surrounding the tumor, is increasingly acknowledged as essential for thorough medical analysis. We employed the mask-padding toolkit available on the OnekeyAI platform to systematically expand the manually delineated intratumoral regions of interest (ROIs). Radial expansion was conducted in increments of 2 mm and 3 mm to systematically assess the impact of varying peritumoral margins on the predictive performance and accuracy of our radiomics model.

Radiomics Procedure

Feature Extraction

A total of 3,745 radiomics features (RFs) were extracted from the defined regions of interest (ROIs) using the ITK-SNAP software (version 3.8.0). This extensive feature set included 890 gray-level co-occurrence matrix (GLCM) features, 740 first-order statistics, 570 gray-level dependence matrix (GLDM) features, 660 gray-level run length matrix (GLRLM) features, 660 gray-level size zone matrix (GLSZM) features, 190 neighborhood gray-tone difference matrix (NGTDM) features, and 35 shape-based features. Notably, texture-related features constituted approximately three-quarters of the total feature pool, highlighting their significant role in the quantitative characterization of tumor heterogeneity.

ITK-SNAP is an open-source software package specifically designed for medical image segmentation, originally developed by Paul Yushkevich and his research team at the University of Pennsylvania. This platform is built upon the Insight Toolkit (ITK) and SimpleITK frameworks, facilitating the interactive visualization and structural segmentation of two-, three-, and four-dimensional medical imaging data, including computed tomography (CT) and magnetic resonance imaging (MRI).

Feature Selection

The robustness of the extracted radiomics features was rigorously assessed. Since feature calculation is inherently reliant on the delineation of tumor sub-regions, only those features exhibiting high stability against segmentation uncertainty were selected for further analysis. Analyses of test-retest and inter-rater reliability were performed to evaluate feature robustness.

For the test-retest analysis, 30 patients were randomly selected from the discovery dataset, and one rater conducted two separate segmentations of the tumor sub-regions for each patient. In the inter-rater analysis, a different cohort of 30 randomly selected patients was utilized, with two independent raters performing the segmentations. The consistency of the features extracted from these multiple segmentations was assessed using the Intraclass Correlation Coefficient (ICC). Features with an ICC of 0.85 or higher were deemed highly robust against both inter- and intra-observer variability.

Following the robustness assessment, dimensionality reduction was conducted to remove highly correlated features. Spearman correlation coefficients were computed for all feature pairs. For any pair exhibiting a correlation coefficient of 0.90 or higher, only one feature was retained to reduce redundancy. Ultimately, 37 radiomic features were selected, ensuring that the final feature set was robust, predictive, and non-redundant.

Signature Building

Radiomics Signature: Utilizing LASSO for rigorous feature selection, we developed a radiomics risk model through machine learning algorithms, including Logistic Regression, Support Vector Machine, and Random Forest. We conducted comparative analyses to assess the performance of each model and examined the advantages of feature fusion by integrating multi-modal features. This approach enabled us to investigate the benefits of combining various imaging modalities to improve predictive accuracy.

Peri Radiomics Signature (PeriXmm): In this context, 'X' represents the distance from the peritumoral region. We employed the same stringent feature selection process as that used for the Intra Radiomics Signature. The final model was developed using a consistent array of machine learning algorithms, thereby ensuring comparability between our analyses of intra- and peri-tumoral regions.

Metrics

The diagnostic efficacy of our deep learning model was rigorously assessed in the test cohort through the construction of Receiver Operating Characteristic (ROC) curves, which evaluated its discriminative ability. Model calibration was analyzed using calibration curves, supplemented by the Hosmer-Lemeshow goodness-of-fit test to confirm its reliability. Furthermore, Decision Curve Analysis (DCA) was utilized to evaluate the clinical utility of our predictive models, thereby enhancing understanding of their potential benefits in a clinical context.

Statistical Analysis

The normality of clinical features was assessed using the Shapiro-Wilk test. Continuous variables were analyzed with either the t-test or the Mann-Whitney U test, depending on their distribution characteristics. Categorical variables were evaluated using Chi-square (χ^2) tests. The baseline characteristics across all cohorts are presented in Table 1. Importantly, p-values greater than 0.05 between cohorts suggested no significant differences, thereby confirming an unbiased division between groups.

All data analyses were executed on the OnekeyAI platform version 4.9.1 utilizing Python 3.7.12. Statistical assessments were conducted with Statsmodels version 0.13.2. Radiomics feature extraction was performed via PyRadiomics version 3.0.1. Machine learning implementations,

including the Support Vector Machine (SVM), were facilitated using Scikit-learn version 1.0.2. Our deep learning frameworks were developed on PyTorch version 1.11.0, optimized for enhanced performance through CUDA version 11.3.1 and cuDNN version 8.2.1.

Table 1
baseline characters of our cohorts.

feature_name	-label = ALL	-label=test	-label=train	pvalue
weight	59.90 ± 9.77	59.59 ± 9.71	60.03 ± 9.81	0.587
BMI	22.16 ± 3.26	22.12 ± 3.19	22.17 ± 3.30	0.856
WBC	6.86 ± 2.96	6.48 ± 1.96	7.03 ± 3.29	0.872
HGB	123.04 ± 28.13	119.57 ± 29.06	124.55 ± 27.67	0.212
RDW_SD	48.34 ± 20.07	49.86 ± 31.04	47.68 ± 12.70	0.374
CHE	6040.44 ± 2173.99	5770.17 ± 2065.53	6158.28 ± 2215.14	0.082
IBIL	9.33 ± 5.36	10.22 ± 5.88	8.94 ± 5.08	0.078
CK	111.12 ± 159.50	105.29 ± 97.62	113.66 ± 180.15	0.555
Mg	0.84 ± 0.09	0.82 ± 0.10	0.84 ± 0.09	0.291
PT	12.23 ± 1.61	12.23 ± 1.68	12.23 ± 1.58	0.897
PTR	1.41 ± 5.79	1.04 ± 0.13	1.57 ± 6.94	0.874
AFP	16.55 ± 108.78	5.59 ± 16.40	21.34 ± 129.73	0.817
diabetes				0.828
0	227(91.90)	68(90.67)	159(92.44)	
1	20(8.10)	7(9.33)	13(7.56)	
surgical_h				0.951
0	167(67.61)	50(66.67)	117(68.02)	
1	80(32.39)	25(33.33)	55(31.98)	
smoke				1.0
0	163(65.99)	49(65.33)	114(66.28)	
1	84(34.01)	26(34.67)	58(33.72)	
T				0.722
2	29(11.74)	7(9.33)	22(12.79)	
3	197(79.76)	61(81.33)	136(79.07)	
4	21(8.50)	7(9.33)	14(8.14)	
M				0.363
0	238(96.36)	74(98.67)	164(95.35)	
1	9(3.64)	1(1.33)	8(4.65)	

Results

Clinical Features

Univariable Analysis: In this study, we conducted a comprehensive univariate analysis of all clinical features, focusing on the calculation of Odds Ratios (OR) and corresponding p-values for each variable. This ratio was instrumental in the development of our final fusion model. Significant features identified through univariable screening were utilized in constructing the Clinical Signature.

In the univariate analysis, various clinical, biochemical, and hematological indicators exhibited significant associations with the Lauren classification. The subsequent multivariate regression analysis revealed that tumor T-stage, cholinesterase (CHE), body weight, and white blood cell (WBC) count serve as independent clinical predictors.

Table 2
Univariable Analysis of clinical features.

feature_name	OR_UNI	OR lower 95%CI_UNI	OR upper 95%CI_UNI	p_value_UNI	OR_MULTI	OR lower 95%CI_MULTI	OR upper 95%CI_MULTI	p_value_MULTI
CHE	1	1	1	0	1.0	1.0	1.0	0.031
CK	1.003	1.001	1.005	0.021	0.999	0.997	1.001	0.32
HGB	1.007	1.005	1.009	0	1.011	0.998	1.025	0.174
weight	1.014	1.01	1.019	0	0.88	0.824	0.94	0.001
RDW_SD	1.019	1.013	1.025	0	0.992	0.969	1.014	0.525
BMI	1.042	1.028	1.054	0	1.245	1.033	1.502	0.055
PT	1.082	1.058	1.107	0	1.159	0.927	1.449	0.277
IBIL	1.088	1.055	1.121	0	1.024	0.95	1.103	0.608
WBC	1.099	1.06	1.14	0	0.877	0.794	0.969	0.03
AFP	1.172	1.089	1.261	0	1.006	0.987	1.025	0.601
T	1.411	1.281	1.554	0	3.255	1.632	6.495	0.005
surgical_h	2.235	1.383	3.611	0.006	0.518	0.252	1.063	0.132
diabetes	2.25	0.837	6.044	0.177				
PTR	2.477	1.891	3.245	0	1.041	0.836	1.297	0.762
smoke	2.625	1.619	4.255	0.001	1.366	0.645	2.895	0.494
M	3	0.783	11.496	0.178				
Mg	3.064	2.199	4.272	0	0.928	0.028	30.356	0.972

Signature Comparison

The Combined model that combines radiomics with clinical features exhibited enhanced performance, attaining an AUC of 0.77 and an accuracy of 0.84. This result suggests that radiomic features extracted from enhanced CT images offer substantial predictive value for the Lauren classification of gastric cancer.

In the training cohort, the Combined model, which integrates radiomics and clinical features, demonstrated the highest accuracy (0.84) and area under the receiver operating characteristic curve (AUC, 0.77), indicating that amalgamating multi-dimensional features significantly bolstered the model's resilience. A slight decrease in performance was noted in the test cohort, possibly due to the limited sample size or potential overfitting.

The IntraPeri model, derived solely from radiomic features of contrast-enhanced CT images, demonstrated a consistent AUC of approximately 0.73, highlighting the considerable discriminative ability of imaging phenotypes for Lauren classification. Although the standalone clinical model showed limited predictive capability, its combination with radiomic data offered significant incremental value, thereby enhancing the overall predictive performance.

Table 3
Metrics on different signature.

Signature	Accuracy	AUC	95% CI	Sensitivity	Specificity	PPV	NPV	Cohort
Clinic	0.496	0.582	0.4526–0.7117	0.415	0.8	0.886	0.267	train
IntraPeri	0.731	0.735	0.6220–0.8478	0.766	0.6	0.878	0.405	train
Combined	0.84	0.773	0.6652–0.8803	0.915	0.56	0.887	0.636	train
Clinic	0.923	0.604	0.0000–1.0000	0.958	0.5	0.958	0.5	test
IntraPeri	0.846	0.594	0.0000–1.0000	0.875	0.5	0.955	0.25	test
Combined	0.385	0.5	0.1332–0.8668	0.333	1	1	0.111	test

ROC curves for various models were analyzed in both the training and test cohorts. In the training cohort, the combined model demonstrated superior performance (AUC = 0.773, 95% CI 0.665–0.880) compared to the clinical and radiomics-only models. However, all models exhibited

reduced performance in the test cohort, with AUCs ranging from approximately 0.5 to 0.6. This decline suggests limited generalizability, likely attributable to overfitting and the small sample size.

Calibration Curve: The Hosmer-Lemeshow (HL) test quantifies the discrepancy between predicted probabilities and observed outcomes; a lower HL statistic indicates better calibration. Calibration plots for the training and validation cohorts demonstrated strong agreement between predicted probabilities and observed outcomes. In the training cohort, the combined model exhibited the best calibration, closely aligning with the ideal diagonal line, while the clinical-only model slightly overestimated risk at lower probability ranges. In the validation cohort, despite fluctuations attributed to sample heterogeneity, the combined model maintained the most consistent calibration, indicating superior generalization compared to single-source models.

DeLong Test: The DeLong test was conducted on both training and testing sets to assess the statistical significance of differences between models. The results indicated that in the training cohort, both the radiomic model (IntraPeri) and the combined model exhibited significantly higher AUCs compared to the clinical model ($p = 0.019$ and $p = 0.005$, respectively). However, the difference between the combined and radiomic models was not statistically significant ($p = 0.219$). In the validation cohort, none of the pairwise comparisons achieved statistical significance (all $p > 0.05$), suggesting comparable discriminative performance among the models. These findings, along with the calibration analysis, imply that the integration of radiomic features enhances model performance during training while ensuring robust generalization in the test set. Furthermore, radiomics and multimodal fusion significantly surpass the clinical baseline in discriminating outcomes, thereby confirming the added value of imaging features in model development. In the test cohort, no significant differences were noted among the three models, indicating comparable discriminative ability and acceptable generalization following overfitting control.

Clinical Use

Decision Curve Analysis (DCA): Fig. 6 illustrates the decision curve analysis (DCA) for both the training and testing sets. The DCA revealed that the combined model provided the highest net benefit across most threshold probabilities in the training cohort, surpassing both the clinical and radiomic models. In the validation cohort, while the differences among the models diminished, the combined model continued to demonstrate the best overall clinical utility. These findings, along with the calibration and DeLong test results, affirm that the integration of radiomic features enhances the clinical decision-making value and generalizability of the predictive model.

The final nomogram was developed using a combined model that integrates clinical variables (WBC, weight, CHE, and T stage) with the radiomic signature (IntraPeri). Each variable is assigned a specific point value, and the cumulative points reflect an individualized risk probability. Consistent with prior calibration, DeLong, and DCA analyses, the nomogram demonstrated high discriminative power, robust calibration, and significant clinical utility, thereby serving as an effective tool for personalized prediction and clinical decision-making.

Discussion

In this study, we developed and validated a radiomics nomogram for the preoperative prediction of Lauren classification in patients with gastric cancer (GC). The Lauren classification is among the most widely utilized histopathological categorization systems for GC [17], reflecting the tumor's biological behavior as well as the progression of its etiology and epidemiological characteristics. These factors significantly influence prognostic outcomes and the formulation of clinical treatment strategies [35, 36, 37, 38]. As a personalized decision-making tool, the radiomics nomogram offers substantial guidance for tailoring clinical management [39]. Our findings indicate that the integrated radiomics nomogram, which combines both radiomic and clinical features, demonstrates superior predictive potential and clinical utility compared to the standalone clinical model.

Historically, the identification of Lauren subtypes in gastric cancer (GC) has depended significantly on pathological diagnoses conducted by clinical oncologists, which typically necessitate invasive biopsies. Although preoperative endoscopic biopsies are commonplace, the limited volume of tissue specimens often results in a low concordance rate—approximately 64.7%—between biopsy and surgical specimens [38]. In recent years, the rapid advancement of artificial intelligence has encouraged researchers to explore innovative diagnostic and therapeutic paradigms that extend beyond traditional methods. Accurate preoperative Lauren classification is essential for surgical planning; for example, the infiltration of diffuse-type GC frequently extends several centimeters beyond the visible tumor boundaries, requiring a more extensive resection margin (typically 8–10 cm from the tumor edge) [36]. Moreover, patients with the diffuse type generally face poorer prognoses compared to those with the intestinal type [40]. Consequently, precise preoperative prediction is of utmost importance. For this study, mixed and diffuse types were categorized together due to their fundamentally similar clinical manifestations and survival outcomes [41]. Additionally, advanced deep learning models have exhibited robust capabilities in automated feature extraction and self-learning [30, 42, 43]. In comparison to traditional radiomic approaches, deep learning can reduce the complexity and subjectivity associated with manual lesion segmentation, thereby improving analytical efficiency and accuracy [44].

In this study, we extracted intratumoral and peritumoral radiomic features from contrast-enhanced CT slices. LASSO regression analysis identified 37 features as independent predictors. Instead of relying solely on univariate analysis, we constructed and validated a radiomics

nomogram for gastric cancer (GC) patients by integrating these combined radiomic features, which represent the tumor and its microenvironment, with clinical information, including white blood cell (WBC) count, cholinesterase (CHE) levels, body weight, and T-stage. Notably, our model exhibited a superior discriminative capability of 84.0% compared to the concordance rate of traditional biopsy at 64.7%, indicating its potential as a non-invasive adjunct for enhancing diagnostic accuracy. The visualization of our model as a user-friendly nomogram can aid clinicians in predicting individual Lauren classifications and serve as a reference for personalized treatment decisions.

This study presents several intrinsic limitations. First, the manual segmentation of tumor regions of interest (ROIs) on CT images is both labor-intensive and costly; future applications may benefit from the implementation of semi-automated or automated segmentation techniques. Second, the retrospective design of this study, coupled with variations in CT equipment, may introduce minor biases or errors in the experimental results. Third, we exclusively employed arterial phase (AP) CT images. Although this phase effectively captures the blood supply characteristics of the lesion, it lacks the dynamic imaging information available in the portal venous phase (VP) or delayed phase (DP), which may result in the omission of certain histological or functional details, thereby limiting the model's generalizability and clinical applicability. Future research should explore the development of multi-phase fusion radiomics models (AP + VP ± DP) or the incorporation of dynamic enhancement parameters (such as K^{trans}, V_e, etc.) to enhance robustness and interpretability. Finally, as a single-center retrospective analysis, the representativeness of the sample may be constrained. Therefore, multi-center data collection is necessary in future studies to further assess the performance and external validity of our model.

Conclusion

In conclusion, we successfully developed and validated a radiomics nomogram for the preoperative prediction of Lauren classification in patients with gastric cancer (GC). This was achieved by integrating intratumoral and peritumoral radiomic features with key clinical predictors, including T-stage, cholinesterase (CHE), body weight, and white blood cell (WBC) count. The nomogram exhibits strong discriminative performance in differentiating between diffuse-type and intestinal-type GC, thereby serving as a valuable non-invasive tool to enhance personalized clinical management and optimize therapeutic strategies.

Abbreviations

GC gastric cancer

CHE cholinesterase

WBC white blood cell

AUC area under the receiver operating characteristic curve

HL Hosmer–Lemeshow

DCA decision curve analysis

OS overall survival

ROI region of interest

DCE-MRI dynamic contrast-enhanced magnetic resonance imaging

RFs radiomics features

Declarations

Author contributions

HX, WXP and YG: conceptualization and design of the study. HX, YYL and WXP: data extraction and organization. HX, YG, RTS and SC: statistical analyses and interpretations. HX: draft of the manuscript and literature search. SC, RTS and YG: revision of manuscript. FS: supervised the entire study and provided critical review. All authors reviewed and approved the submitted manuscript.

Funding

The Joint Special Project of Yunnan Provincial Department of Science and Technology and Kunming Medical University (NO. 202501AY070001-030).

Data availability

All data generated or analysed during this study are included in this published article [and its supplementary information files].

Ethics approval and consent to participate

This study was approved by **The Medical Ethics Committee of the Second Affiliated Hospital of Kunming Medical University**. The requirement for informed consent to participate was waived by **The Medical Ethics Committee of the Second Affiliated Hospital of Kunming Medical University** due to the retrospective nature of the study and in accordance with relevant institutional and national regulations.

Consent for publication

Not applicable.

Competing interests

The authors declare no competing interests.

Author details

*Correspondence: Feng Sun, e-mail: SunFeng1971@163.com

[1]The Second Ward of Gastrointestinal Surgery Department of the Second Affiliated Hospital of Kunming Medical University, Kunming 650000, China

[2]Kunming Medical University, Kunming 650000, China

[3]*Hang Xiong and Yun Gong contributed equally to this work*

References

1. Zhou YH, Chen XL, Zhang X, et al. Dual-phase contrast-enhanced CT-based intratumoral and peritumoral radiomics for preoperative prediction of lymph node metastasis in gastric cancer[J]. BMC Gastroenterol. 2025;25(1):123.
2. Fatima S, Song Y, Zhang Z, et al. Exploring the pharmacological mechanisms of P-hydroxylcinnamaldehyde for treating gastric cancer: a pharmacological perspective with experimental confirmation[J]. Curr Mol Pharmacol. 2024;17:e18761429322420.
3. Cheng M, Guo Y, Zhao H, et al. CT-based deep learning radiomics analysis for preoperative lauren classification in gastric cancer and explore the tumor microenvironment[J]. Eur J Radiol OPEN. 2025;15:100667.
4. Song J, Xu X, He S, et al. Myristicin suppresses gastric cancer growth via targeting the EGFR/ ERK signaling pathway[J]. Curr Mol Pharmacol. 2023;16(7):712–24.
5. Zhang X, Jin M, Yao X, et al. Upregulation of LncRNA WT1-AS inhibits tumor growth and promotes autophagy in gastric cancer via suppression of PI3K/akt/mTOR pathway[J]. Curr Mol Pharmacol. 2024;17:e18761429318398.
6. Shah MA, Kelsen DP. Gastric cancer: a primer on the epidemiology and biology of the disease and an overview of the medical management of advanced disease[J]. J Natl Compr Cancer Network: JNCCN. 2010;8(4):437–47.
7. Shah MA, Khanin R, Tang L, et al. Molecular classification of gastric cancer: a new paradigm[J]. Clin Cancer Research: Official J Am Association Cancer Res. 2011;17(9):2693–701.
8. Chen YC, Fang WL, Wang RF, et al. Clinicopathological variation of lauren classification in gastric cancer[J]. Pathol Oncol Research: POR. 2016;22(1):197–202.
9. Choi J, Chung H, Kim J, et al. Determining the current indications for endoscopic submucosal dissection in patients with lauren mixed-type early gastric cancer[J]. J Gastroenterol Hepatol. 2020;35(4):586–92.
10. Qiu Mzhen, Cai M, sheng yan, Zhang D, et al. Clinicopathological characteristics and prognostic analysis of lauren classification in gastric adenocarcinoma in China[J]. J Translational Med. 2013;11:58–64.
11. Chia NY, Tan P. Molecular classification of gastric cancer[J]. Annals Oncology: Official J Eur Soc Med Oncol. 2016;27(5):763–9.
12. Shen XM, Zhou C, Lian L, et al. Relationship between the DPD and TS mRNA expression and the response to S-1-based chemotherapy and prognosis in patients with advanced gastric cancer[J]. Cell Biochem Biophys. 2015;71(3):1653–61.
13. Tang CT, Zeng L, Yang J, et al. Analysis of the incidence and survival of gastric cancer based on the lauren classification: a large population-based study using SEER[J]. Front Oncol. 2020;10:1212.
14. Hu SB, Liu CH, Wang X, et al. Pathological evaluation of neoadjuvant chemotherapy in advanced gastric cancer[J]. World J Surg Oncol. 2019;17(1):3.

15. Jiménez Fonseca P, Carmona-Bayonas A, Hernández R, et al. Lauren subtypes of advanced gastric cancer influence survival and response to chemotherapy: real-world data from the AGAMENON national cancer registry[J]. Br J Cancer. 2017;117(6):775–82.
16. Ajani JA, D'Amico TA, Bentrem DJ, et al. Gastric cancer, version 2.2022, NCCN clinical practice guidelines in oncology[J]. J Natl Compr Cancer Network: JNCCN. 2022;20(2):167–92.
17. Lordick F, Carneiro F, Cascinu S, et al. Gastric cancer: ESMO clinical practice guideline for diagnosis, treatment and follow-up[J]. Annals Oncology: Official J Eur Soc Med Oncol. 2022;33(10):1005–20.
18. Oue N, Sentani K, Sakamoto N, et al. Molecular carcinogenesis of gastric cancer: lauren classification, mucin phenotype expression, and cancer stem cells[J]. Int J Clin Oncol. 2019;24(7):771–8.
19. Röcken C. Predictive biomarkers in gastric cancer[J]. J Cancer Res Clin Oncol. 2023;149(1):467–81.
20. Ma L, Xu X, Zhang M, et al. Dynamic contrast-enhanced MRI of gastric cancer: correlations of the pharmacokinetic parameters with histological type, lauren classification, and angiogenesis[J]. Magn Reson Imaging. 2017;37:27–32.
21. Liu S, Liu S, Ji C, et al. Application of CT texture analysis in predicting histopathological characteristics of gastric cancers[J]. Eur Radiol. 2017;27(12):4951–9.
22. Lambin P, Rios-Velazquez E, Leijenaar R, et al. Radiomics: extracting more information from medical images using advanced feature analysis[J]. Eur J Cancer. 2012;48(4):441–6.
23. Aerts HJWL, Velazquez ER, Leijenaar RTH, et al. Decoding tumour phenotype by noninvasive imaging using a quantitative radiomics approach[J]. Nat Commun. 2014;5:4006.
24. Gillies RJ, Kinahan PE, Hricak H. Radiomics: images are more than pictures, they are data[J]. Radiology. 2016;278(2):563–77.
25. Lambin P, Leijenaar RTH, Deist TM, et al. Radiomics: the bridge between medical imaging and personalized medicine[J]. Nat Rev Clin Oncol. 2017;14(12):749–62.
26. Sun KY, Hu HT, Chen SL, et al. CT-based radiomics scores predict response to neoadjuvant chemotherapy and survival in patients with gastric cancer[J]. BMC Cancer. 2020;20(1):468.
27. Jiang Y, Liang X, Wang W, et al. Noninvasive prediction of occult peritoneal metastasis in gastric cancer using deep learning[J]. JAMA Netw Open. 2021;4(1):e2032269.
28. Jiang Y, Zhang Z, Yuan Q, et al. Predicting peritoneal recurrence and disease-free survival from CT images in gastric cancer with multitask deep learning: a retrospective study[J]. Lancet Digit HEALTH. 2022;4(5):e341–50.
29. Dong D, Fang MJ, Tang L, et al. Deep learning radiomic nomogram can predict the number of lymph node metastasis in locally advanced gastric cancer: an international multicenter study[J]. Annals Oncology: Official J Eur Soc Med Oncol. 2020;31(7):912–20.
30. Li J, Dong D, Fang M, et al. Dual-energy CT-based deep learning radiomics can improve lymph node metastasis risk prediction for gastric cancer[J]. Eur Radiol. 2020;30(4):2324–33.
31. Dong D, Tang L, Li ZY, et al. Development and validation of an individualized nomogram to identify occult peritoneal metastasis in patients with advanced gastric cancer[J]. Annals Oncology: Official J Eur Soc Med Oncol. 2019;30(3):431–8.
32. Zhang W, Fang M, Dong D, et al. Development and validation of a CT-based radiomic nomogram for preoperative prediction of early recurrence in advanced gastric cancer[J]. Radiotherapy Oncology: J Eur Soc Therapeutic Radiol Oncol. 2020;145:13–20.
33. Zhang L, Dong D, Zhang W, et al. A deep learning risk prediction model for overall survival in patients with gastric cancer: a multicenter study[J]. Radiotherapy Oncology: J Eur Soc Therapeutic Radiol Oncol. 2020;150:73–80.
34. Wang S, Feng C, Dong D, et al. Preoperative computed tomography-guided disease-free survival prediction in gastric cancer: a multicenter radiomics study[J]. Med Phys. 2020;47(10):4862–71.
35. Lakhani P, Sundaram B. Deep learning at chest radiography: automated classification of pulmonary tuberculosis by using convolutional neural networks[J]. Radiology. 2017;284(2):574–82.
36. Hundahl SA, Phillips JL, Menck HR. The national cancer data base report on poor survival of U.S. gastric carcinoma patients treated with gastrectomy: fifth edition american joint committee on cancer staging, proximal disease, and the different disease hypothesis[J]. Cancer. 2000;88(4):921–32.
37. Ansari S, Gantuya B, Tuan VP, et al. Diffuse gastric cancer: a summary of analogous contributing factors for its molecular pathogenicity[J]. Int J Mol Sci. 2018;19(8):2424.
38. Qiu MZ, Shi SM, Chen M, et al. Comparison of HER2 and lauren classification between biopsy and surgical resection samples, primary and metastatic samples of gastric cancer[J]. J Cancer. 2017;8(17):3531–7.
39. Wang XX, Ding Y, Wang SW, et al. Intratumoral and peritumoral radiomics analysis for preoperative lauren classification in gastric cancer[J]. Cancer Imaging: Official Publication Int Cancer Imaging Soc. 2020;20(1):83.
40. Satoh A, Shuto K, Okazumi S, et al. Role of perfusion CT in assessing tumor blood flow and malignancy level of gastric cancer[J]. Dig Surg. 2010;27(4):253–60.

41. Lauren P. The two histological main types of gastric carcinoma: diffuse and so-called intestinal-type carcinoma. An attempt at a histo-clinical classification[J]. Acta Pathologica et Microbiol Scand. 1965;64:31–49.
42. Peng H, Dong D, Fang MJ, et al. Prognostic value of deep learning PET/CT-based radiomics: potential role for future individual induction chemotherapy in advanced nasopharyngeal carcinoma[J]. Clin Cancer Research: Official J Am Association Cancer Res. 2019;25(14):4271–9.
43. Hu Y, Xie C, Yang H, et al. Computed tomography-based deep-learning prediction of neoadjuvant chemoradiotherapy treatment response in esophageal squamous cell carcinoma[J]. Radiotherapy Oncology: J Eur Soc Therapeutic Radiol Oncol. 2021;154:6–13.
44. Zhu Y, Man C, Gong L, et al. A deep learning radiomics model for preoperative grading in meningioma[J]. Eur J Radiol. 2019;116:128–34.

Figures

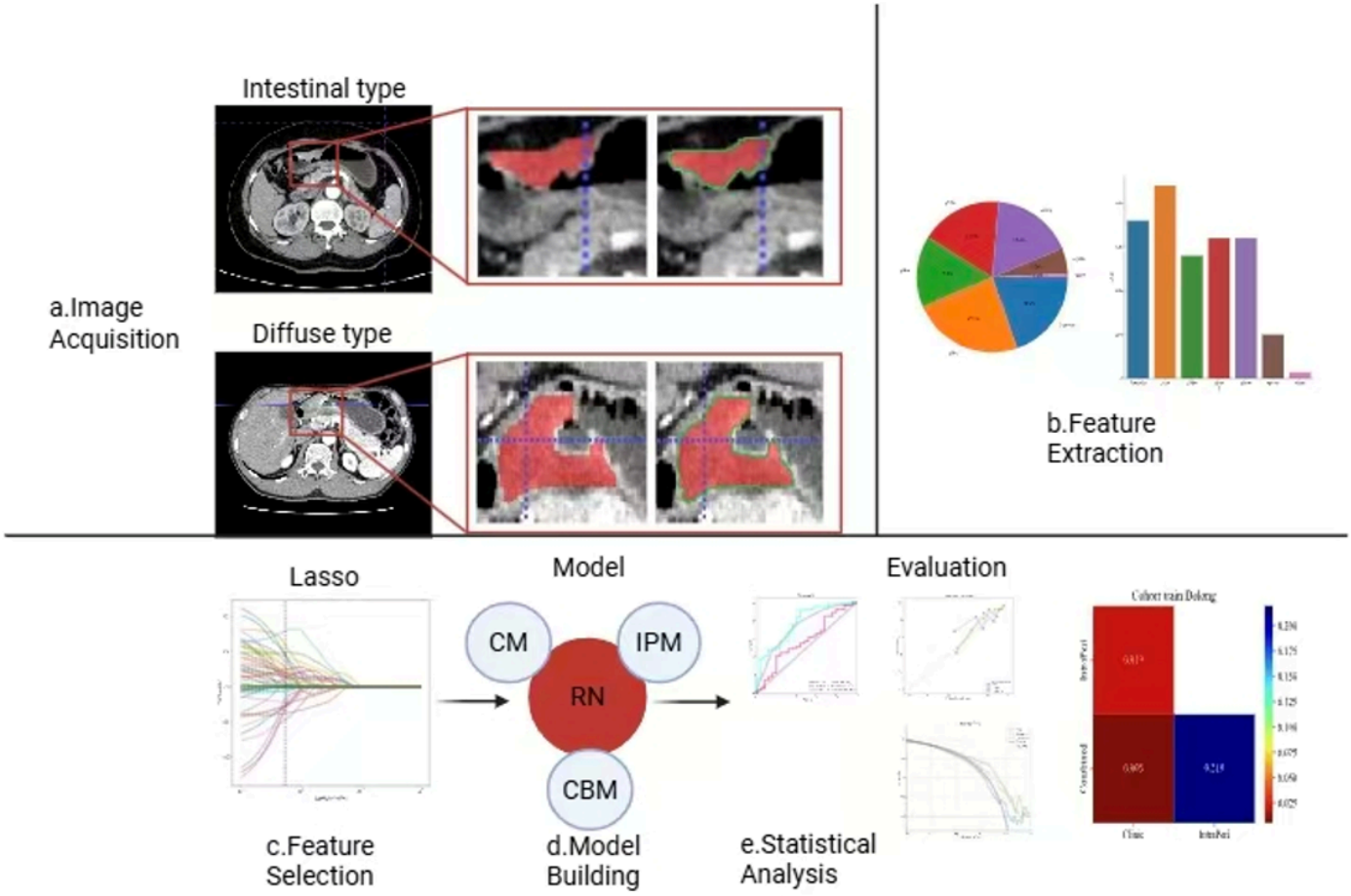


Figure 1

Workflow of this study. LASSO, least absolute shrinkage and selection operator; RN, radiomic nomogram; CM, clinical model ; IPM, IntraPeri model(integrating intratumoral and peritumoral radiomics features)，CBM, Combined model (integrating radiomics and clinical features).

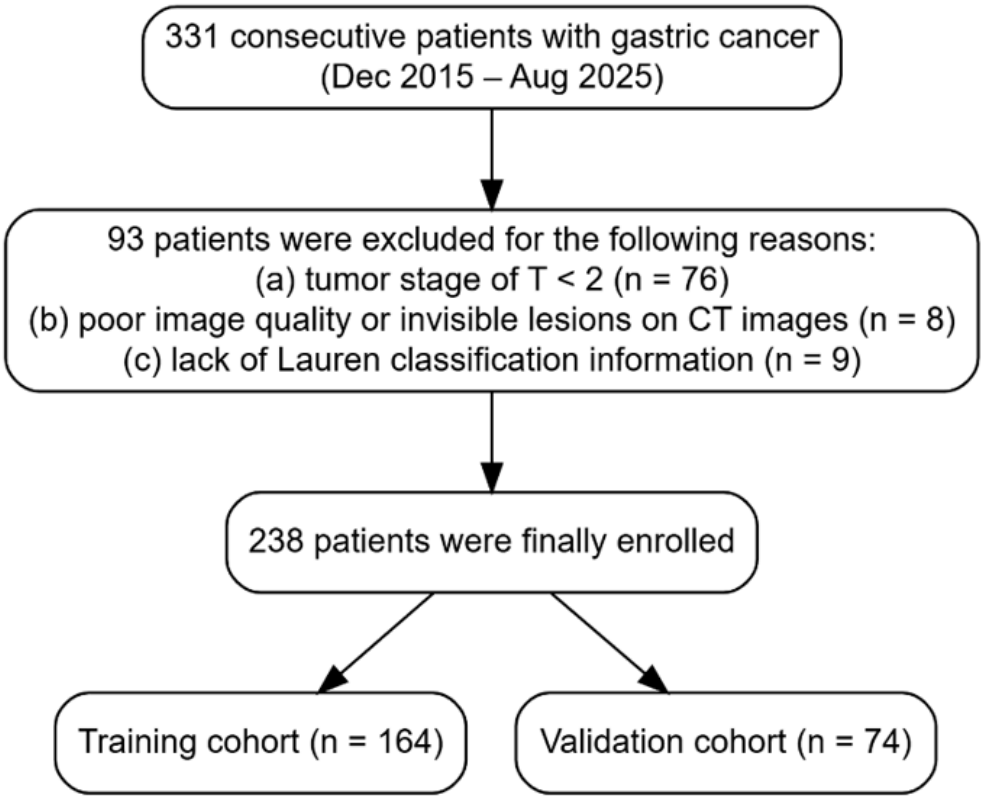


Figure 2

Flow Chart

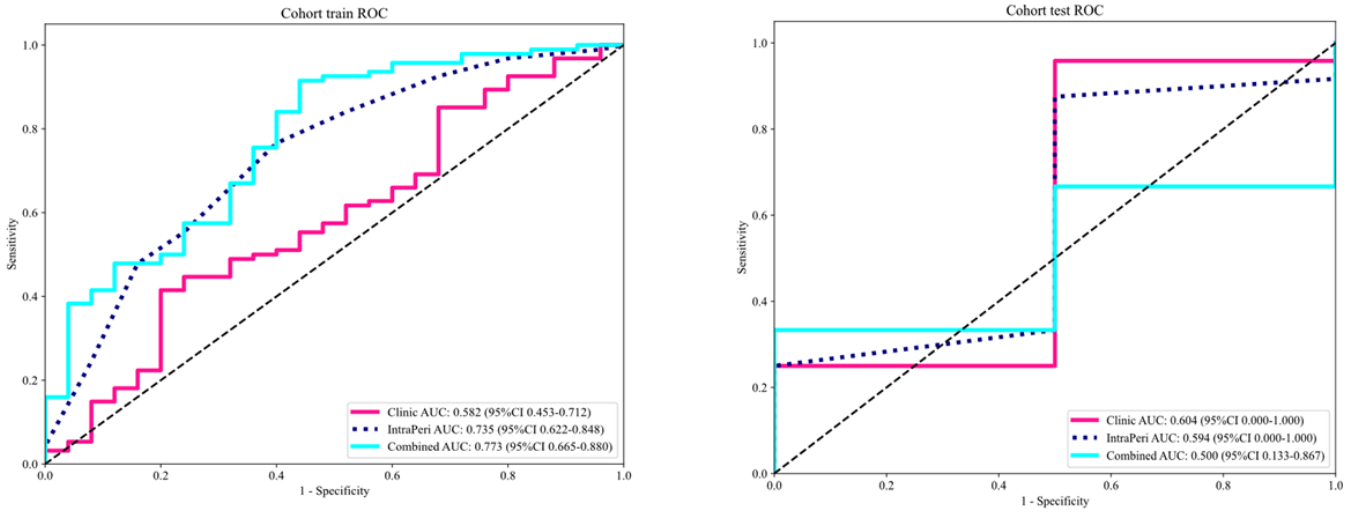


Figure 3

Different signatures' ROC on different cohort.

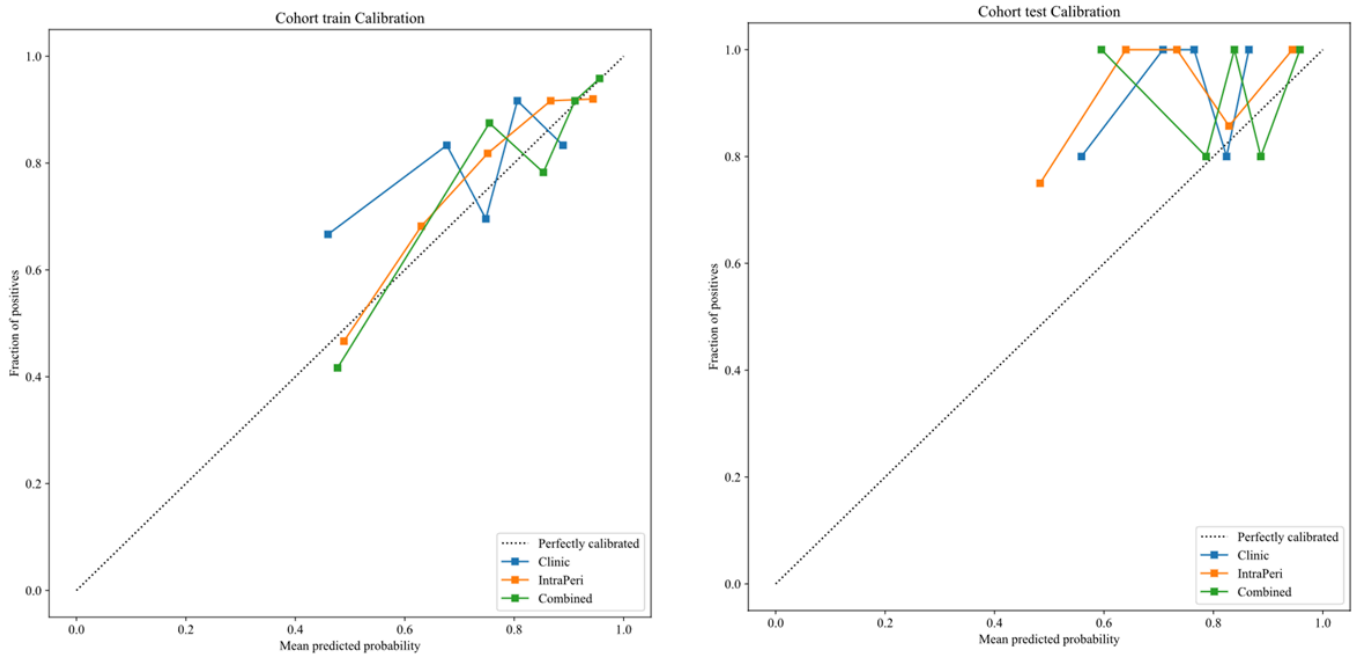


Figure 4

Calibration curves of different signatures for the test cohort.

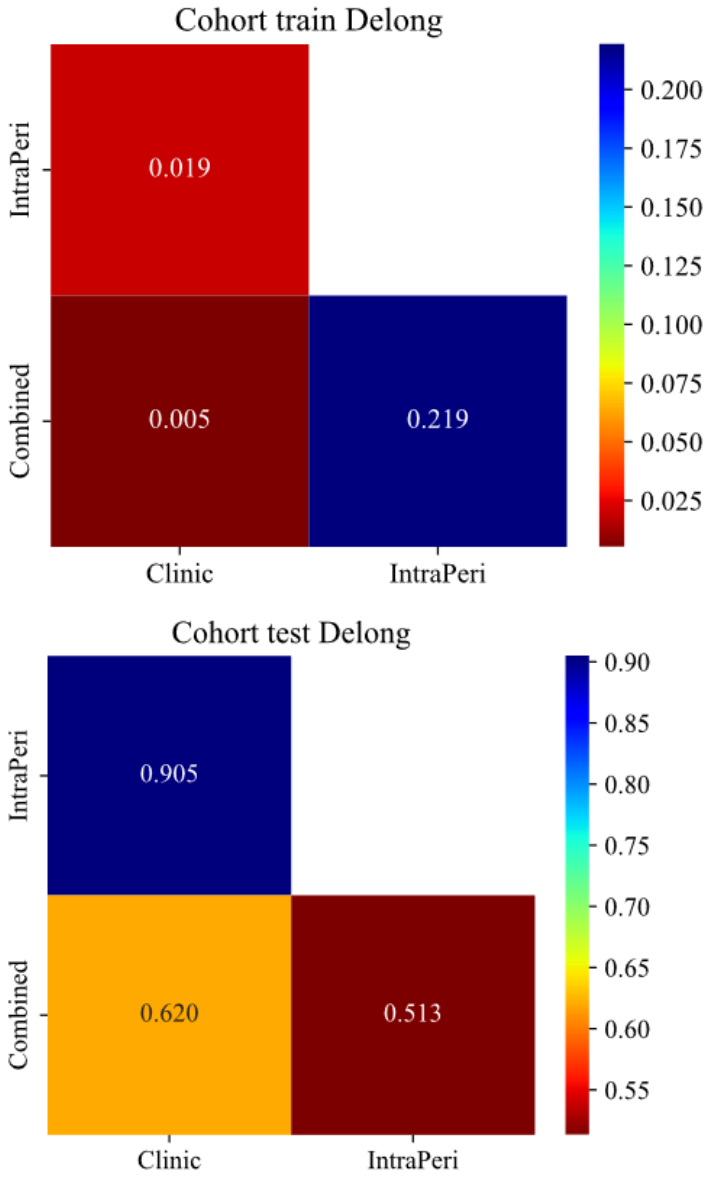


Figure 5

DeLong test results for different signatures.

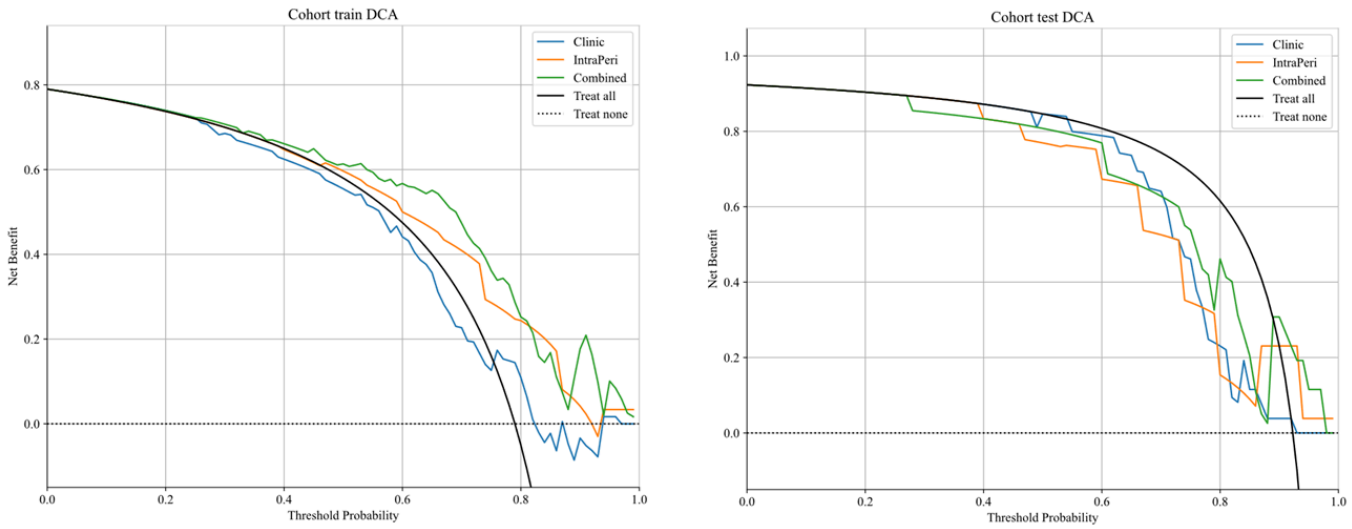


Figure 6

Different signatures' decision curve on test cohort.

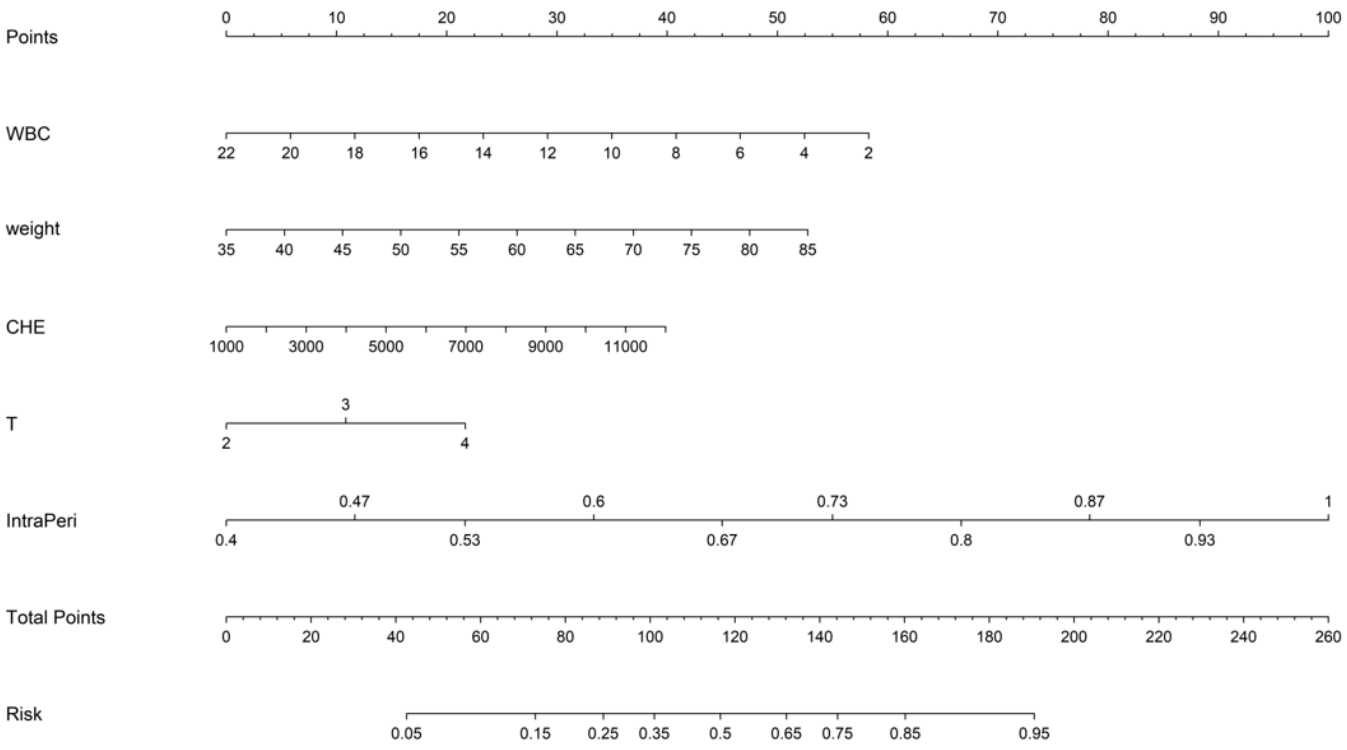


Figure 7

Unnumbered image in the Result section.

Supplementary Files

This is a list of supplementary files associated with this preprint. Click to download.

- supplementaryinformationfiles.zip